

Opera suspicionată (OS)
Suspicious work**Opera autentică (OA)**
Authentic work

OS	Raveica, I.C., Schnakovszky, C., „Studies concerning the contact between two asperities in deforming and milling process”, <i>Annals of the Oradea University. Fascicle of Management and Technological Engineering, Volume VII (XVII)</i> , p.1746-1752, 2008.
OA	Boucly, V., Nélias, D., Green, I., „Modeling of the Rolling and Sliding Contact Between Two Asperities”, <i>Journal of Tribology</i> , Vol. 129, p.235-245, April 2007.

Incidența minimă a suspiciunii / Minimum incidence of suspicion

p.1746:07 – p.1746:14	p.235:04 – p.235:07; p.235:12 – p.235:17
p.1746:25 – p.1747:09	p.235:29s – p.235:43s
p.1747:10 – p.1747:11	p.235:07d – p.235:09d
p.1747:14 – p.1747:18	p.235:19d – p.235:24d
p.1747:19 – p.1747:24	p.236:07s – p.236:14s
p.1747:26 – p.1748:03	p.236:16s – p.236:50s
p.1748:04 - p.1752:09	p.237:29d - p.240:14s
p.1753:09 – p.1753:25	p.244:05s – p.244:27s

Fișa întocmită pentru includerea suspiciunii în Indexul Operelor Plagiate în România de la www.plagiate.ro

STUDIES CONCERNING THE CONTACT BETWEEN TWO ASPERITIES IN DEFORMING AND MILLING PROCESS

Ionel Crinel, RAVEICA¹, Carol SCHNAKOVSKY²

⁽¹⁾University of Bacău, Faculty of Engineering e-mail: ravic@ub.ro, ⁽²⁾University of Bacău, Faculty of Engineering e-mail: scarol@ub.ro

Keywords: machining process, contact modeling, elastic-plastic contact, tangential and normal loading

Abstract: The paper presents A semi-analytical method for the tridimensional elastic-plastic contact between two hemispherical asperities The first part of the paper describes the algorithm used to deal with the normal contact, which can be either load-driven or displacement-driven (dd). The contact pressure distribution, the hydrostatic pressure and the equivalent plastic strain state below the contacting surfaces are also found to be strongly modified in comparison to the case of an elastic-plastic body in contact with a purely elastic body. The way to consider rolling and sliding motion of the contacting bodies consists of solving the elastic-plastic contact at each time step while upgrading the geometries as well as the hardening state along the moving directions.

1. INTRODUCTION

The process presented in this paper consists in combined three elementary processes: cold plastically deformation on superficial layer, aiming to obtain a hardening structure; conventional milling of deformed layer and finally, settling and cold hammering process [6]. The final aspects of surface is presented in Fig. 1 .

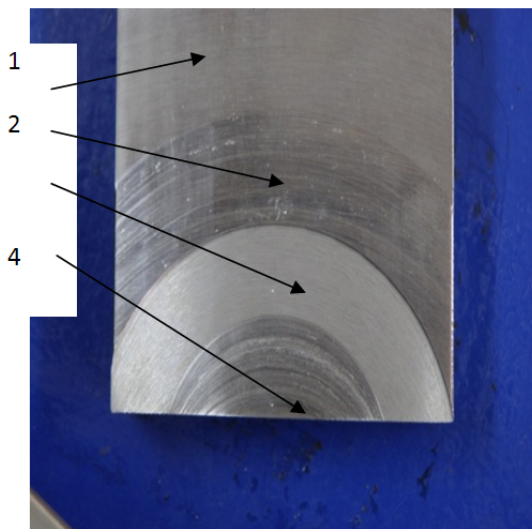


Fig.1 The instant aspect of processed surface. 1-classic milled surface 2-rolled surface 3- conventional milling surface of deformed layer 4 -the settled surface.

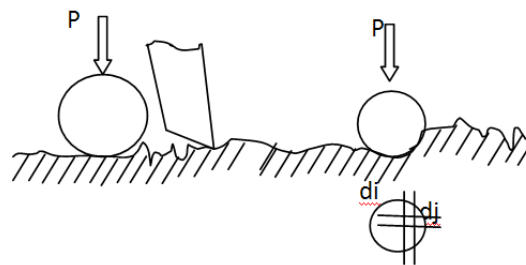


Fig.2 The instant aspect of deforming and milling process

Concerning the goal of this new process, the manufacturing method can be exposed in Fig. 2, where the three elementary processes are shortly represented.

Starting from this point we observe that in this case can found on superficial layer elastically deformation, elasto-plastically deformation and plastically deformation, on asperities level.

It is now well recognized that semi-analytical methods are efficient methods for solving contact problems. Compared to finite element analyses, semi-analytical methods

show much shorter computation times, typically by several orders of magnitude. In SAM, analytical formulas are derived using Green functions, commonly called influence coefficients in the discrete form. Quantities are then obtained by numerical computing using accelerating techniques, leading to extremely short computation times. Among many numerical methods it seems that the most efficient to solve contact problem are the conjugate gradient method first introduced by Polonsky and Keer [1], the multi-level multisummation technique first implemented by Lubrecht and Ioannides [2], the fast Fourier transform introduced by Ju and Farris [3] and used by Nogi and Kato for contact problems with layers [4].

The first part of the paper is focused on the simulation of the normal contact, which is the first step in the modeling of asperities tugging in simple sliding motion.

It should be pointed out that the displacement-driven (dd) formulation is well adapted to the localized contact between two opposite asperities since the load distribution between asperities for real rough surfaces is not known a priori. The way to consider rolling and sliding motion of the contacting bodies consists of solving the elastic-plastic contact at each time step while upgrading the geometries as well as the hardening state along the moving directions. An application to the tugging between two spherical asperities in simple sliding (dd formulation) is made in the second part of the paper.

The current paper focuses only on the mechanical deformation involved in sliding contact in order to uncouple the phenomenon. Compared to previous researchers' models, the proposed method can be applied either to statistical or deterministic approaches, in order to study the rolling and sliding thermal-elastic-plastic contact between real 3D rough surfaces. It is to be noted that the bodies in contact can follow any hardening law; i.e., they are not restricted to be perfectly plastic.

2. LOAD-DRIVEN (ld) VERSUS DISPLACEMENT-DRIVEN (dd) FORMULATIONS

In order to simulate the rolling/sliding contact, a ld formulation was first used by applying a normal load (vertical loading) prior to the tangential displacement of the load (rolling load). In such a formulation one may consider a frictionless contact, as well as the effect of friction, which often tends to overload the near-surface area. This formulation is well adapted when considering the whole contact between two bodies pressed against each other with a prescribed load. On the other hand, when focusing the analysis to the contact between two single asperities led on opposite surfaces that are in relative motion, it is clear that this localized interaction is more related to a rigid body displacement (interference) producing a transient normal and tangential loading when asperities collide. It should be noted that the tangential load is here defined as the force that acts opposite to the relative velocity, which is not limited to frictional effects since the contact surface is barely parallel to the relative velocity between the contacting surfaces. This is the reason a friction coefficient is purposely omitted in this study; i.e., in order to uncouple tangential effects induced by mechanical deformations, and the ones induced by friction. The mechanism at the origin of the tangential load found when two asperities tug each other is similar to the one found during ploughing when a normally loaded rigid indenter is translated on the surface of a deformable media.

A realistic application of the sliding between two asperities with a fixed value of the interference could be the sliding of a projectile between two rails in an electromagnetic launcher for example, since the projectile is sliding on two rails that are fixed in distance.

Basically the load-driven formulation shows very good results in terms of convergence rate and accuracy, but the user is forced to fix a value for the load, resulting in finding a rigid body displacement after computation. As said earlier, this is convenient

for the resolution of the whole contact, but not to describe the tugging between two single asperities. Thereafter, the contact algorithm for the displacement-driven formulation is presented.

In the case of the contact between an elastic-plastic body and a rigid punch (nano-indentation test), the load-driven formulation has been validated with the finite element software ABAQUS, and also experimentally, see [5]. For this simulation, the elastic-plastic body is a flat made of steel used in aeronautic applications. The elastic properties of this steel are $E=210$ GPa for the Young modulus, and $\nu =0.3$ for Poisson ratio. The Swift law is used to describe the hardening behavior, see Eq. [1] and the chosen parameters are $B=1240$ MPa, $C=30$, and $n=0.085$. It is to be noted that the equivalent plastic strain in this expression is expressed in microdef (10^{-6} def). These values are taken corresponding to the experimental data presented in [5].

$$\sigma_{VM} = B(C + e^p)^n \quad (1)$$

For the rigid punch, a sphere with radius $105 \mu\text{m}$ is chosen (nanoindenter tip). The load is progressively applied until 0.650 N and then the two bodies are unloaded until the contact no longer occurs.

Figures 3 and 4 present a comparison between the load-driven and the displacement-driven formulations. Figure 3 gives the evolution of the load versus the interference during loading and unloading. It is observed here the influence of both plasticity and conformity change due to permanent deformation of the surface, since the curves are really different for the loading and the unloading phases. Plasticity is a phenomenon that depends on the loading history.

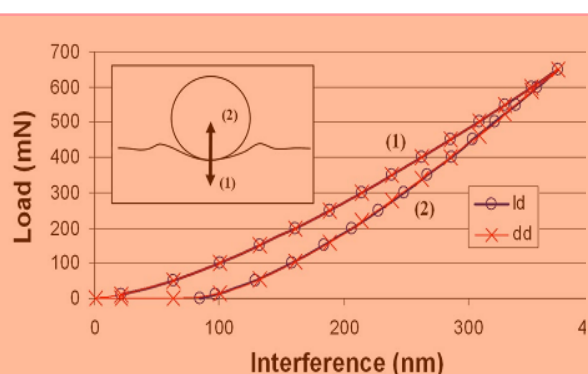


Fig. 3 Load (mN) versus interference during the loading/unloading phases. Max load 0.650 N/Max interference 372 nm.

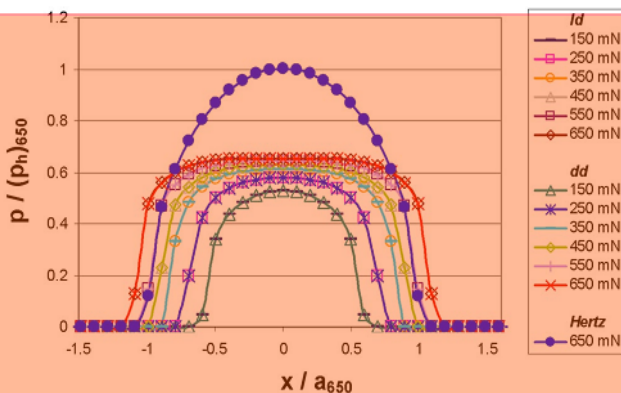


Fig. 4 Pressure distribution at the end of the loading phase, in the plane $y=0$. Load 0.650 N

The pressure distribution in the plane $y=0$ (longitudinal plane) for an increasing load is given in Fig. 4. The pressure distribution is found flattened compared to the Hertz solution. This is due mostly to hardening of the elastic-plastic material, which tends to increase the contact area. There is also a little influence of the geometry change due to permanent deformation of the surface.

As it can be seen, a very good agreement is found, for a comparable time computation with for the mesh-size, $dx=0.6\mu\text{m}$, $dy=1.2\mu\text{m}$, $dz=0.3\mu\text{m}$, i.e., $31 \times 17 \times 44 = 23,188$ points in the plastic zone and with a total of 26 time-step increments for

loading/unloading _about 25 min for the whole loading/unloading process on a 1.8 GHz Pentium® M personal computer.

3. MODELING OF THE CONTACT BETWEEN TWO ELASTIC-PLASTIC BODIES

This paragraph deals with the contact between two elastic-plastic bodies. The current assumptions are that the two bodies have the same initial geometry with identical elastic properties and hardening behavior. In order to validate the new proposed algorithm, a comparison with a finite element simulation is made through the normal contact between two spheres. The differences between the case of an elastic-plastic body in contact with another elastic-plastic body, and the case of an elastic-plastic body in contact with a pure elastic body will be outlined [7].

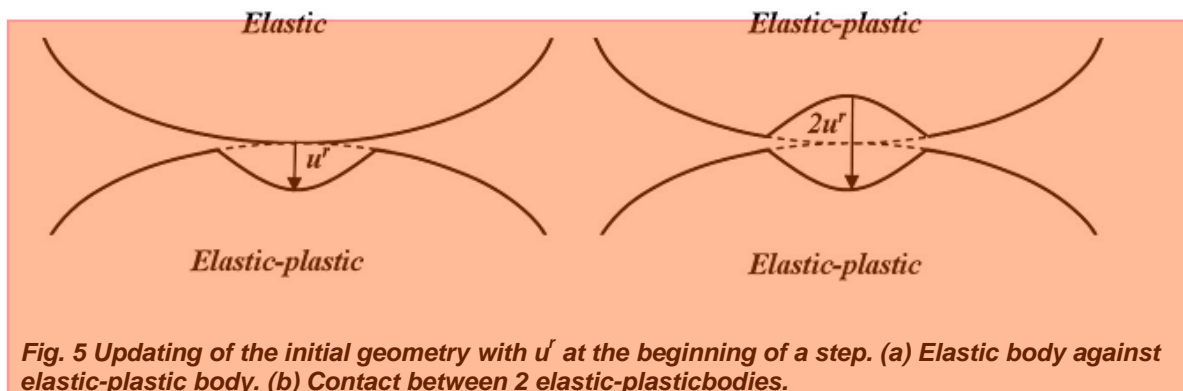
3.1 Improved Algorithm. The algorithm has been improved to deal with two elastic-plastic bodies in contact. The only change in the previous models is in Eq. (2)., when the initial geometry is updated, it takes into account the change in both bodies geometry at the same time since h_{ij} is actually the surface separation. At the beginning of each new increment, the pressure is calculated, and this pressure repartition is applied on both counter surfaces. The residual displacement calculated at the end of the increment is then added to the initial geometry. If one of the bodies is elastic, then the residual displacement is basically added to the initial geometry (see Fig. 5).

$$h_{ij} \leftarrow h_{ij} + u'_{ij} \quad (2)$$

Though, if the bodies are both elastic-plastic and have the same hardening behavior, then the surface separation in Eq. (2) becomes

$$h_{ij} \leftarrow h_{ij} + 2u'_{ij} \quad (3)$$

because of the symmetry about the plane of contact (see Fig. 5).



3.2 Results. A simple example is proposed that corresponds to the simulation of the normal contact between two spheres of radius 15 mm. The spheres are made of Rul 99 bearing steel, with elastic properties $E=210$ GPa for the Young modulus, and $\nu=0.3$ for the Poisson ratio. The hardening law is described by a Swift law, as in Eq. (1), with parameters $B=945$ MPa, $C=20$, and $n=0.121$. Here again, ep is expressed in microdef. In order to compare the results for the loaded case, Fig. 5 shows the pressure repartition at

the end of the loading with a normal load of 11,179 N, corresponding to a Hertzian pressure of 8 GPa.

The pressure P is normalized by the Hertzian pressure P_h , and the abscissa x by the Hertzian contact radius a . The axisymmetric FE model consists of 40,247 elements _type CAX4R_ with 81,128 degrees of freedom. Two EP (Elastic-Plastic) situations are presented, the first one with only one inelastic body (E_EP), the second one when both bodies are inelastic (EP_EP, with the same hardening law). As can be seen, a very good agreement is observed between the results provided by ABAQUS and the ones from the semi-analytical code (SAC).

In order to compare the results for the unloaded case, Fig. 6 shows this time the evolution of the hydrostatic pressure

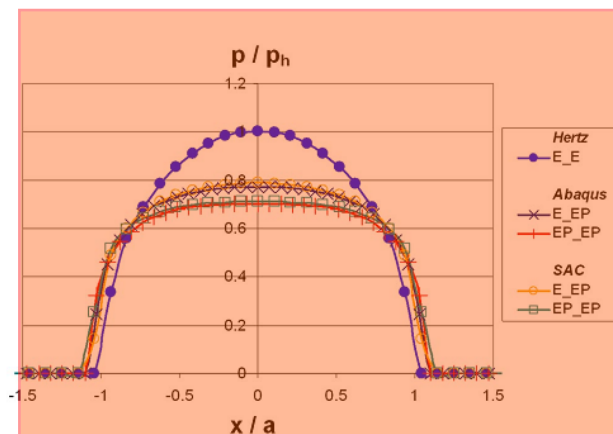


Fig. 6 Pressure distribution at the end of loading in the plane $y=0$. Load 11,179 N, i.e., $P_h=8$ GPa and Hertzian contact radius $a=817 \mu\text{m}$.

as defined in Eq. (3) versus the depth, in the same conditions as before; i.e., at the end of the loading and with the same hardening law. Again, the hydrostatic pressure is normalized by the Hertzian pressure P_h , and the depth z by the hertzian contact radius a .

$$P_{hydro} = \frac{1}{3}(\sigma_1^r + \sigma_2^r + \sigma_3^r) \quad (4)$$

with $\sigma_1^r, \sigma_2^r, \sigma_3^r$, the principal components of the residual stress tensor.

As it can be seen again, a very good agreement is observed between the results provided by Abaqus and the ones from the SAC.

One may observe two regions where the residual stress state is compressive: at the Hertzian depth and at the surface, whereas two tensile regions are found: one between the surface and the Hertzian depth, but very close to the surface, and one far below the Hertzian depth.

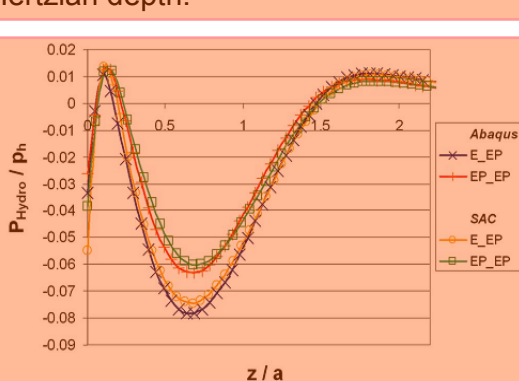


Fig. 7 Hydrostatic pressure at the end of loading at the center of the contact. Load 11,179 N, i.e., $P_h=8$ GPa, and Hertzian contact radius $a=817 \mu\text{m}$

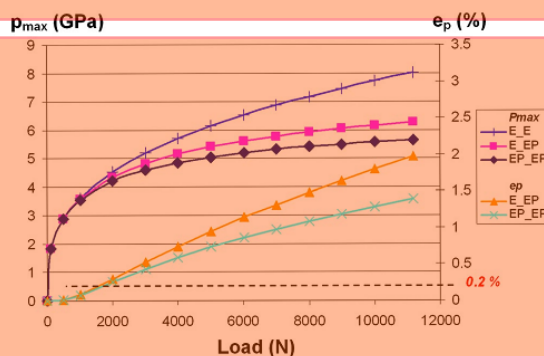


Fig. 8 Maximum contact pressure P_{max} (GPa) and equivalent plastic strain e_p (%) versus the normal load (N)

One may also observe that the maximum compressive value is found at depth $z/a = 0.68$; i.e., deeper than the Hertzian depth ($z/a = 0.48$) Almost no variation difference is found in the tensile zones, whereas an important difference in the compressive zone at the Hertzian depth is found, the minimum value being smaller when one of the bodies is considered as elastic. Figure 7 gives the maximum contact pressure and the corresponding maximum equivalent plastic strain versus the normal load at the center of the contact. The dash line indicates the plasticity threshold in terms of equivalent plastic strain commonly used to define the yield stress, i.e., $\epsilon_p = 0.2\%$, that will be used later to define the critical load at the onset of yielding. To find the aforementioned critical value, a polynomial interpolation is used

$$P^L(x) = \sum_{j=1}^n P_j^L(x) \tag{5}$$

where x is equal to 0.2%, and where P_j^L are the Lagrange polynoms expressed as follows

$$P_j^L(x) = y_j \prod_{k \neq j} \frac{x - x_k}{x_j - x_k} \tag{6}$$

where x_j are the values of the equivalent plastic strains, and y_j the values of the loads. One obtains then for the critical loads, $L_c = 1649$ N for the case of the contact between an elastic and an elastic-plastic bodies, and $L_c = 1743$ N for the case of the contact between two elastic-plastic bodies. The latter value will be used in what follows to present now the same results in a dimensionless form, see Fig. 9 the maximum contact pressure P_{max} being normalized by the Hertz pressure P_h and the normal load L by the critical load $L_c = 1743$ N. An increasing difference between the two curves with increasing load can be seen. As in Fig. 8 one may also observed a pronounced reduction of the maximum contact pressure when considering two EP bodies compared to a purely elastic one against an EP one, up to 11% at the highest load (see Fig. 10).

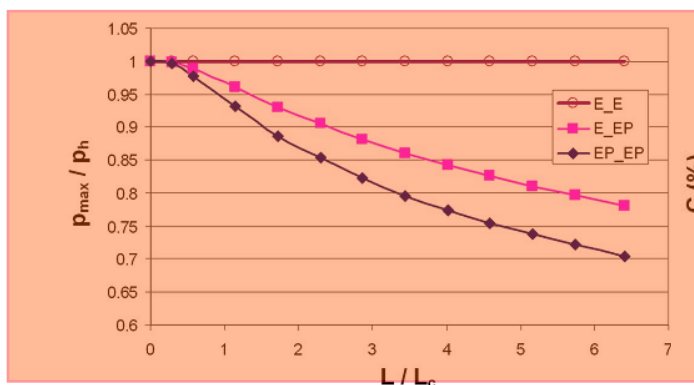


Fig. 9 Dimensionless contact pressure versus dimensionless load found at the center of the contact

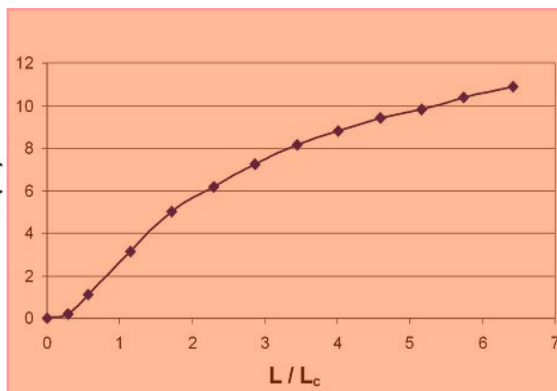


Fig. 10 Difference between the maximum contact pressures obtained assuming an E_EP and EP_EP behavior versus the dimensionless load L/L_c

Another interesting trend in Fig. 9 is the discrepancy between the EP response compared to the Hertz solution, at the critical load; i.e., $L/L_c = 1$. Whereas the analysis remains within the classical assumption of elastic behavior, since the plastic strain ϵ_p does not exceed 0.2%, it appears that the real contact pressure is 5% lower than the Hertz

solution when considering two EP bodies. Note that the difference between the E_EP and the EP_EP solutions is given in Fig. 10 in terms of percentage as defined by Eq. (7)

$$C(\%) = \frac{P_{max}^{E_EP} - P_{max}^{EP_EP}}{P_{max}^{EP_EP}} 100 \quad (7)$$

From Fig. 10 it can be concluded that for $L/L_c < 1$, i.e., 4.5 GPa for the Hertzian pressure, the error made is less than 3%, if only one body behaves inelastically compared to two identical EP bodies in contact. It should be also noticed that, if two different elastic-plastic hardening laws are considered for the bodies in contact, the difference between the E_EP and EP_EP solutions will be lowered, making more appropriate the simplification of considering the harder material as purely elastic.

4. Experimental results on hardening relate to deforming and milling process [6]

The modeling of elasto-plastic hemispheres in contact with a rigid surface is important in contact mechanics on both the macro and micro scales. There is ambiguity and a lack of a universal definition of hardness. Not only are there various hardness tests for various scales and materials (Brinell, Rockwell, Vickers, Knoop, Shore, etc.) defines hardness as "Resistance of metal to plastic deformation, usually by indentation. However, the term may also refer to stiffness or temper, or to resistance to scratching, abrasion, or cutting. It is the property of a metal, which gives it the ability to resist being permanently, deformed, broken, or have its shape changed, when a load is applied. The greater the hardness of the metal, the greater resistance it has to deformation.

Evolution of Deformation

As long as the deformations are purely elastic, i.e., below the critical interferences, the entire hemisphere will abide to 3D Hooke's law. Conforming to Poisson's effect, the material volume should compress with a compressive contact pressure. To investigate this phenomenon the radial deformation of the last contact point between the deformed hemisphere and the rigid flat as extracted from the FEM postprocessing data. Indeed at relatively small values there seems to be a shrinkage in volume even though that some plastic deformation has already taken place, but overall the elastic deformation of the entire hemisphere dominates!. At values below critical interferences, the radial displacements are all negative, very small, and are generally strength independent. In plasticity, however, volume is conserved. As the deformation increases, the yielded material flows plastically and is incompressible, making Poisson's ratio effectively equal to 0.5. The FEM results find that beyond critical displacement, the radial deformation of the last contact point displaces positively. The positive displacement becomes material dependent, which increases with material strength.

Stress Distribution and Evolution

Initially, at small interferences, the sphere will deform only elastically. While in the elastic regime, the maximum von Mises stress will always occur beneath the contact surface and within the bulk material. Eventually, as the interference increases and the stresses increase, yielding will initiate at the point of maximum von Mises stress.

At interferences just above the critical, the plastically deformed region is small and confined below the surface by a sizeable region of elastic material. It should be noted that because of plotting resolution the region of plastic deformation is smaller than the highest stress region shown in each plot. For instance, the highest stress region has a von Mises stress range between 1.444 and 1.624 GPa, and thus not the entire region in this stress range is at the yield stress of 1.619 GPa. With increasing interference, the plastic region

expands until it reaches the surface of the sphere. From close inspection of postprocessing data, according to the current model, the interference at which the plastically deformed region first reaches the surface is approximately when critical interference $\omega=9.6$, (this differs from the value $\omega=6$ as reported by Kogut and Etsion experiments). The value of ω also varies slightly with the material yield strength and the deformed contact geometry for the same reason that the average pressure or hardness varies with strength.

5. CONCLUSION

For modeling an elastic-plastic rolling/sliding contact, a tridimensional elastic-plastic code has been adapted, requiring some specific developments. A new formulation has been proposed to drive the computation by imposing a normal rigid body displacement also called contact interference. Thanks to the use of optimized numerical techniques, which are the conjugate gradient and the discrete convolution and fast Fourier transform, the computation time remains very reasonable in comparison to similar but 2D only analysis performed by FEM, and despite a large number of points in the plastic zone. The contact between two identical elastic-plastic bodies has been first analyzed. A significant reduction of the contact pressure compared to the situation when a purely elastic body is in contact with an elastic-plastic one has been shown. In order to complete the study, the tugging between two single asperities has then been investigated. Results have shown that plasticity produces an asymmetry of the normal and tangential loading during the transient contact. A load ratio due to ploughing has been estimated. Compared to finite element modeling, the developed code allows the user to compute a rolling and sliding contact in very short CPU times. The current work provides the foundation to incorporate electrical-mechanical interaction between rough surfaces by progressively introducing the relevant physical phenomena.

REFERENCES

- [1] Jacq, C., Nélias, D., Lormand, G., and Girodin, D., 2002, "Development of a Three-Dimensional Semi-Analytical Elastic-Plastic Contact Code," ASME J. Tribol., **124**, pp. 653–667.
- [2] Ju, Y., and Farris, T. N., 1996, "Spectral Analysis of Two-Dimensional Contact Problems," ASME J. Tribol., **118**, pp. 320–328.
- [3] Lubrecht, A. A., and Ioannides, E., 1991, "A Fast Solution of the Dry Contact Problem and the Associated Sub-Surface Stress Field, Using Multilevel Techniques," ASME J. Tribol., **113**, pp. 128–133.
- [4] Nogi, T., and Kato, T., 1997, "Influence of a Hard Surface Layer on the Limit of Elastic Contact—Part I: Analysis Using a Real Surface Model," ASME J. Tribol., **119**, pp. 493–500.
- [5] Polonsky, I. A., and Keer, L. M., 1999, "A Numerical Method for Solving Rough Contact Problems Based on the Multi-Level Multi-Summation and Conjugate Gradient Techniques," Wear, **231**, pp. 206–219.
- [6] Raveica, I.C. 2007, Considerații teoretice și experimentale privind procedeul de prelucrare prin deform-frezare, Teza de doctorat, Universitatea Politehnică București.
- [7] Raveica I.C., Gherghel M, Minciu C., (2006) *Mathematical Modeling Of Tool Wearing In Case Of Frontal Finishing Milling Of Grey Cast Iron Fc200* Machinebuilding and Tehnosphere tom3 pag126-29,Sevastopol Ukraina